IEEE Access
Multidisciplinary | Rapid Review | Open Access Journal

Received June 28, 2020, accepted July 27, 2020, date of publication July 31, 2020, date of current version August 11, 2020.

Digital Object Identifier 10.1109/ACCESS.2020.3013394

A Deep Learning-Based Method for Heat Source Layout Inverse Design

JIALIANG SUN[1], JUN ZHANG[2], (Associate Member, IEEE), XIAOYA ZHANG[2], (Member, IEEE), AND WEIEN ZHOU[2]

[1]College of Aerospace Science and Engineering, National University of Defense Technology, Changsha 410073, China
[2]National Innovation Institute of Defense Technology, Chinese Academy of Military Science, Beijing 100071, China

Corresponding author: Weien Zhou (weienzhou@outlook.com)

This work was supported by the National Natural Science Foundation of China under Grant 51675525 and Grant 11725211.

ABSTRACT Heat source layout design is an effective technique to enhance the thermal performance in the whole system, which has become a vital part in many engineering fields, e.g. satellite layout design and integrated circuit design. Traditionally, the optimal design is obtained by searching the design space with the optimization technique which repeatedly runs the thermal simulation to compare the performance of each scheme. Due to the extremely large computational burden with this method, the optimization is greatly limited. To overcome the challenge, heat source layout inverse design (HSLID) is proposed in this article to directly generate the layout scheme with the given thermal performance requirement. A novel method for heat source layout inverse design, denoted as SAR-HSLID, is proposed based on the recently deep learning technique, Show Attend and Read (SAR) model. Firstly, regarding the mapping from the required temperature field to layout scheme as an image-to-location task, this article introduces SAR model, which is good at sequence predicting, to generate the layout scheme. The trained SAR is capable of learning the underlying physics of the design problem, thus can efficiently predict the design under given requirement without any physical simulation. Secondly, to ensure that the designed heat source layout exactly satisfies the input temperature field requirement, based on the layout predicted by SAR, we further utilize a simple but efficient optimization process to conduct few post-processing. Finally, a heat source layout inverse design task in a typical two-dimensional heat conduction problem is investigated to demonstrate the feasibility and effectiveness of the proposed method.

INDEX TERMS Heat source layout design, inverse design, show, attend and read model, deep learning.

I. INTRODUCTION

Heat source layout design (HSLD) is encountered in many fields of engineering and science, particularly in the electronics [1]. The objective of HSLD is to design the reasonable source layout scheme to offer the expected thermal environment for the whole system. With the increasingly smaller size of components and higher power intensity, HSLD has become a critical problem for the development of many fields such as microelectronic technology or satellite design [2]. However, most existing approaches for solving HSLD are based on optimization techniques, in which a large amount numerical simulation of temperature distribution is integrated into the optimization loop [3]–[5]. Besides, with the problem becoming complex or the mesh of simulation being highly refined, the calculation cost would further increase, and it is more difficult to optimize. To alleviate the challenge, one possible solution is by use of heat source layout inverse design (HSLID). The objective of HSLID is to directly design the reasonable layout scheme with the expected themal performance given.

In a typical inverse design problem [6], parameters or layout are sought to achieve the expected system outcomes. For the heat source layout inverse design problem, the objective is to directly design a reasonable layout scheme when the expected thermal performance is given. Then the cost of physical simulation would be reduced greatly. Though there exist no reports about inverse method for heat source layout design, there are some research in other fields. Examples of inverse problems can be found in material design [7], [8], structure

The associate editor coordinating the review of this manuscript and approving it for publication was Yuan Zhuang.

optimization [9], determination of radiative properties of the medium [10], model parameter estimation [11], and image synthesis [12]. Most existing methods for solving inverse problems are based on optimization techniques, which could be classified into two categories: evolutionary algorithms [13], [14] and adjoint method [15]. The first category searches the design space step by step, which takes a lot of computational cost with the increasing parameters. The second category is more efficient than evolutionary algorithms, however, which requires a deep knowledge in physics and can be quite nontrivial.

However, apart from the aforementioned traditional methods for solving inverse problem, some deep learning methods increasingly attract researchers' attentions due to its great success in image classification [16], natural language processing (NLP) [17], object detection [18], PDE solver [19], [20] and image restoration [21] *et al.* One major advantage of deep learning based method is that it could learn the hidden relationship between high-dimensional data and nonlinear model, which is difficultly dug by the traditional methods. Therefore, some deep learning models have been applied in many traditional design areas such as mechanical design [22]–[27], optics [28], [29], fluid simulation [30], [31], biomedical science [32], [33] and materials [34]. For example, in the area of mechanical design, Sosnovik and Oseledets [22] constructed a convolutional encoder-decoder network to predict the optimal design from the intermediate design schemes obtained during evolution, which greatly accelerates the process of topological optimization (TO). Yu *et al.* [23] firstly proposed a method to learn a mapping from boundary conditions/loading conditions to a low resolution optimal structure in TO by using variational autoencoder (VAE). A two-level generative adversarial network (GAN) was constructed by Chen *et al.* [24] to generate shapes who can possess hierarchical dependency with keeping the inter-part dependencies satisfied. Zhang and Ye [25] utilized the VAE model to learn the the constraints and generate design candidates that automatically satisfy all the constraints in TO. Chen *et al.* [26] used the Feature Pyramid Network (FPN) model to learn the mapping from the heat source layout to temperature field as a surrogate to reduce the cost of optimization. The deep convolutional neural network was first utilized by Hamouche and Loukaides [27] to identify the manufacturing process that formed a part solely from the final geometry. In optics, Peurifoy *et al.* [28] utilized artificial neural networks to approximate light scattering by multilayer nanoparticles, which could be used to solve nanophotonic inverse design problems. In fluid simulation, Tompson *et al.* [30] proposed a data-driven approach that they trained a well-tailored convolutional neural network (CNN) to replace the solution of the sparse linear system in the standard fluid solvers. In biomedical science, Liu *et al.* [32] and Han *et al.* [33] also made some work of predicting the mechanical properties based on deep learning. Agrawal *et al.* [34] proposed a systematic end-to-end framework to explore materials informatics based on predictive model such as neural network. From these, it could be concluded that they substitute the entire or intermediate design process by use of the strong learning capability of deep learning in data.

In view of the above successful applications of deep learning technique in other design areas or inverse problems, it is also possible to solve heat source layout inverse design by use of deep learning. However, VAE or GAN in previous work are not suitable for heat source layout inverse design. One major reason is that both of them are generative model, which could not guarantee the final output meet the layout shape or other constraints in HSLD. In addition, both of them also need additional post-processing. However, Show Attend and Read (SAR) [35] could help to overcome this challenge well if treating the heat source layout design as an image-to-location task. SAR is an important and efficient technique in deep learning. It uses a simple but effective neural network model augmented with 2D attention that aims to utilize the most salient features in image. It is applied popularly in natural language processing to solve irregular text recognition problem. The motivation of selecting SAR other than VAE or GAN is that the heat source layout share the similar features with the layout of text. The ouputs of them are all discrete layout sequence, which means that we do not need any post-processing to make the shape constraints or overlapping constraints be meeted. Meanwhile, we found that it is also appropriate for the task of inverse heat source layout design since it can automatically detect where the heat source appears by taking full advantage of the attention mechanism in SAR model.

In this article, we propose a novel inverse method for HSLID based on deep learning. Heat source layout inverse design includes two steps: the design of reasonable temperature field and the design of method for predicting the layout according to the thermal performance. In this article, we mainly focus on the method about inversely predicting the layout according to the temperature field. It means that in the inverse design, the design of temperature field information could not be given arbitrarily. The most ideal circumstance is that we can design a reasonable temperature field according to our need, which corresponds to a known possible items distribution. To realize it, taking the mapping from the temperature field to the heat source layout as an image-to-location task, we construct the SAR model with neural networks and train the model by our pre-generated dataset. The dataset consists the initial layout satisfying the shape constraints and the corresponding temperature field represented by pair images. Experiments show that SAR model could directly design the heat source layout for most expected temperature filed. Based on this, we also design a simple but efficient optimization process to try to ensure the consistency between the layout design and the expected temperature field. Considering real-world applications, we investigate the relationship between the size of temperature field and the predicted accuracy using our proposed method. Experiments show the competitive performance of our method in dealing

with HSLID. In summary, the contributions of our paper are three-folds:

1) Regarding the mapping from the required temperature field to heat source layout as an image-to-location task, we first introduce SAR model in NLP to solve heat source layout inverse design problem. The trained SAR model could directly generate superior heat source layout schemes that meet our expected thermal performance.

2) Aiming at the few circumstances that the thermal performance of heat source layout scheme designed by SAR does not satisfy the expectation, we design a simple but efficient optimization process to conduct few post-processing.

3) Requirement of few measurement points in real world impels us to investigate the relationship between the size of temperature field and the performance of the proposed method. Experiments show that our method stays competitive even though with ten times smaller input size.

The remainder of this article is structured as follows. In Section II, the mathematical model of heat source layout inverse design problem is established. In Section III, a SAR-based framework of HSLID is proposed. In Section IV, the predicted performance of the trained SAR model is evaluated by the predefined accuracy metric and also how the training data size influences the accuracy is investigated. Finally, the conclusion and future research prospects are discussed in Section V.

II. PROBLEM DESCRIPTION

In this section, heat source layout inverse design problem is investigated. Given an expected temperature field $\boldsymbol{X}$, the objective is to inversely determine the heat sources position $\boldsymbol{Y}$. The thermal performance of $\boldsymbol{Y}$ should keep consistency with the expected $\boldsymbol{X}$ as much as possible. Thus its solution can be reduced to an optimization problem as follows:

$$\begin{cases} \text{find} & \boldsymbol{Y} \\ \text{minimize} & J(x,y) = max|\mathbf{T_p}(\mathbf{x},\mathbf{y}) - \mathbf{X}(\mathbf{x},\mathbf{y})_k| \\ & (k = 1, 2, 3 \ldots n) \\ \text{s.t.} & \Gamma_i \cap \Gamma_j = \emptyset \quad \forall i \neq j \\ & \Gamma_i \subset \Gamma_0 \quad \forall i = 1, 2, \ldots, N_s \end{cases} . \quad (1)$$

where (x, y) stands for the positions of measure points in the temperature field, T_p stands for the temperature field of heat source layout designed by inverse method based on deep learning, n represents the number of measurement points in the whole temperature field, Γ_i represents the covering area of the ith heat source, Γ_0 denotes the layout domain area and N_s is the total number of heat sources.

To solve Eq.(1), we need heat simulation to obtain the value of $\mathbf{T_p}(\mathbf{x}, \mathbf{y})$ after designing the heat source layout inversely. It is because that the value of $\mathbf{T_p}(\mathbf{x}, \mathbf{y})$ involves the solution of the corresponding Poisson's equation. The steady-state temperature field (T) in a two-dimensional plane induced by a number of heat sources can be calculated by solving the Poisson's equation as follows:

$$\begin{gathered} \frac{\partial}{\partial x}\left(k\frac{\partial T}{\partial x}\right) + \frac{\partial}{\partial y}\left(k\frac{\partial T}{\partial y}\right) + \phi(x,y) = 0 \\ T = T_0 \quad \text{or} \quad k\frac{\partial T}{\partial \mathbf{n}} = 0 \quad \text{or} \quad k\frac{\partial T}{\partial \mathbf{n}} = h\,(T - T_0) \end{gathered} \quad (2)$$

where T means the thermal conductivity of the layout domain and $\phi(x, y)$ represents the intensity distribution function describing heat sources. In the boundary conditions of the governing equation, T_0 is the temperature at the isothermal boundary and h means the convective heat transfer coefficient.

Actually, Eq.(2) presents a Poisson's equation with three different boundary conditions: Dirichlet (isothermal), Neumann (adiabatic) or Robin (convective). Poisson's equation does not have explicit representation. So it could not be solved directly by gradient-based methods. Thus people usually use heat simulation for estimation approximately.

The intensity distribution function $\phi(x, y)$ is determined by the positions of heat sources, which can be expressed as

$$\phi(x,y) = \begin{cases} \phi_0, & (x,y) \in \Gamma \\ 0, & (x,y) \notin \Gamma \end{cases} \quad (3)$$

where ϕ_0 is the intensity of one single heat source and Γ denotes the layout area covered by the heat source.

In this article, we take a general volume-to-point (VP) heat conduction problem as an example. Multiple heat sources are placed in a rectangular domain. Then we are to inversely design the heat source layout to meet the expected thermal performance.

As previously defined in [3]–[5], the VP problem with heat sources distributed in a square domain is illustrated in Figure 1. All the boundaries of this domain are adiabatic except one tiny heat sink (T_0) in the middle of the bottom boundary. Obviously, the investigated HSLID in this article is a two-dimensional Poisson's problem with mixture of Dirichlet and Neumann boundary conditions.

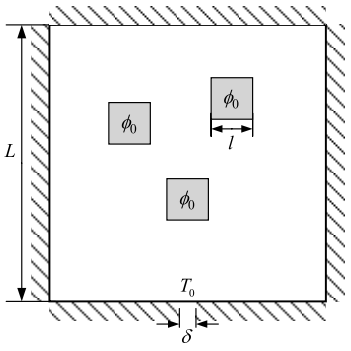

FIGURE 1. The VP problem in a square domain.

III. THE FRAMEWORK OF SAR-HSLID

As described in section I, the solution of HSLD demands the computation of physical simulation. The simulation cost would increase greatly with more complicated heat source layout. In addition, when the number of heat source increases,

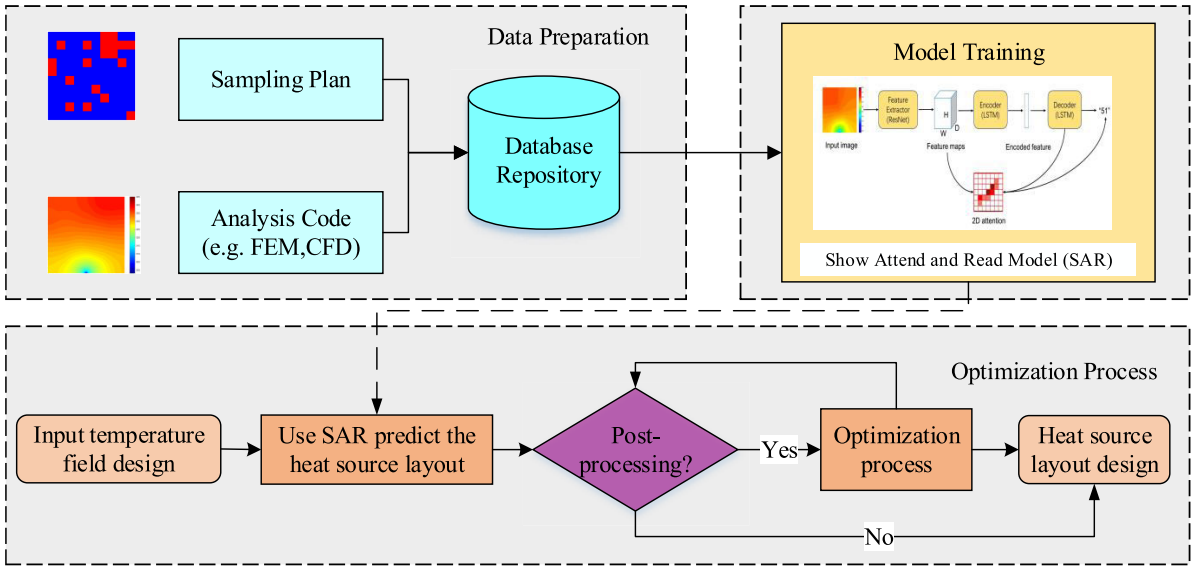

FIGURE 2. The illustration of SAR-HSLID framework.

it is difficult to solve for existing optmization method based on evolutionary algorithms such as Genetic Algorithm (GA). To cope with these difficulties, we propose a novel inverse method for HSLID based on SAR. Whatever complicated the layout scheme is, SAR could still possess competitive performance by treating it as a image-to-location regression problem. Then taking the layout scheme outputed by SAR as the initial layout scheme, we introduce an optimization process to conduct few post-processing, denoted as SAR-HSLID, which improves the accuracy compared with the original SAR. SAR-HSLID has three parts: data preparation, model training and optimization process. The brief process of three parts is illustrated in Figure 2.

Data preparation. We generate variant samples randomly as the training data according to the designed sampling strategies. Each sample pair consists of one heat source layout scheme and its corresponding temperature field simulated by Finite Element Method (FEM) or Computational Fluid Dynamics (CFD).

Model training. Taking the layout and the temperature field as source images, the mapping modeling can be regarded as an image-to-location regression task. Regarding this aspect, SAR is utilized to learn the inherent laws of the provided data.

Optimization process. Once the SAR model is constructed, the traditional optimization strategies or algorithms for post-processing can be combined to solve HSLID. Based on the high prediction precision of SAR model, HSLID presented in Section II is investigated.

Next, we introduce each part of SAR-HSLID in detail.

A. DATA PREPARATION

In this article, to validate the performance of our proposed method, the defined problem is similar as [3]–[5], [26]. Detaily, as shown in Figure 4, 20 items that share the same shape 20 × 20 and heat intensity are placed in a 200 × 200 square domain.To simplify the problem, the 200×200 square domain is divided into 10×10. Each item could only be placed and moved in the discrete 20×20 plane. The length of the side of the square layout domain is set as $L = 0.1$m. The thermal conductivity of the domain and the heat source component is $k = 1$ W/(m·K). 20 identical square heat sources are required to be placed in the domain with the side length $l = 0.01$m and the intensity $\phi_0 = 10000\text{W/m}^2$. The width of the narrow heat sink is set as $\delta = 0.001$m and its temperature value is constant at $T_0 = 298$K. When we prepare the data, the layout is represented by a 200 x 200 binary matrix only including 0 or 1, which is illustrated in Figure 5. The layout domain is first divided into 10 x 10 grid uniformly, resulting in 100 cells. Each heat source is only placed on one cell. Then each cell is further divided into 20 x 20 grid, resulting in the 200 x 200 layout domain. Thus the different layout data could be generated by using different integer sequences ranging from 1 to 100 without repeatly. The corresponding temperature field of each layout scheme is numerically calculated by the finite-difference method (FDM) proposed in [36]. The mesh is not uniformly generated where the narrow heat sink region is refined to guarantee the numerical simulation precision.Then we generate general data and special data by taking the different layout schemes as initial seeds, which are displayed in Figure 3. General data is generated by taking the random layout schemes as seeds. Special data is generated by taking the special layout schemes as seeds. Different layout schemes could be obtained by adopting the designed sampling strategy [26]. After obtaining the temperature field, we pre-process the input temperature field by normalizing the value of each point to be beneficial for the training of neural network as follows:

$$T_{input}(x, y) = \frac{T(x, y) - 298}{10} \tag{4}$$

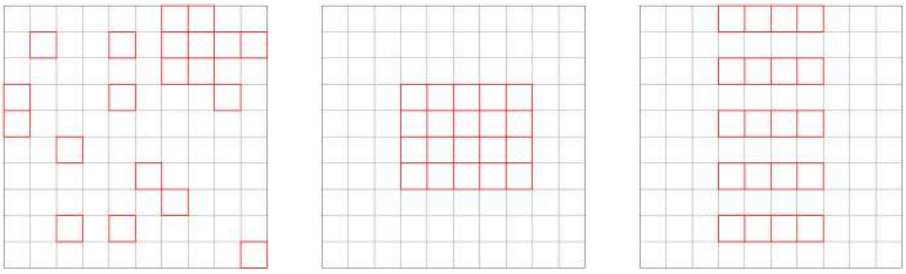

(a) Random layout schemes (b) Special layout schemes (c) Special layout schemes

FIGURE 3. Taking different layout schemes as seeds in the evolving sampling strategy.

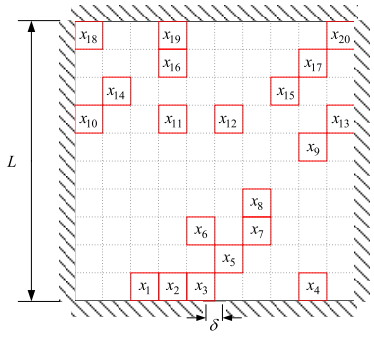

FIGURE 4. The illustration of 20 heat source items layout in a square domain.

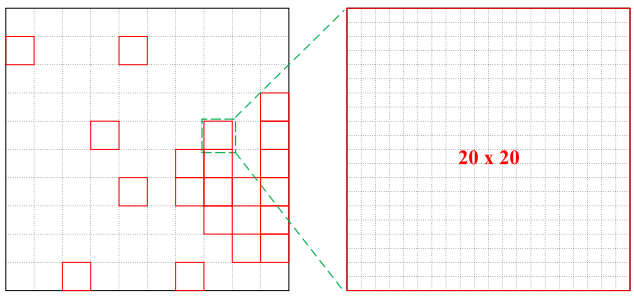

FIGURE 5. The illustration of layout representation. The layout domain is first divided into 10 x 10 uniformly, resulting in 100 cells. Each heat source is only placed on one cell. Then each cell is further divided into 20 x 20 grid, resulting in the 200 x 200 layout domain. The value of cells occupied by heat sources is 1. The value of the other vacant cells is 0.

where $T(x, y)$ represents the temperature value of point (x, y) in the domain, $T_{input}(x, y)$ stands for the corresponding pre-processed temperature value as the input of neural network.

B. LAYOUT REPRESENTATION

Given a temperature field $\boldsymbol{X}$, the SAR model needs to predict its corresponding heat source layout design $\hat{\boldsymbol{Y}}$. The input to the SAR model is a real-valued image $\boldsymbol{X}$ with size 200×200, and the output of SAR is a sequence of positions ended up with a special token [EOS] indicating the end of a sequence: $\tilde{\boldsymbol{Y}} = \{y_1, y_2, \cdots, y_n, [\text{EOS}]\}$, where n is the sequence length and each position y_i is in the range of $\{1, 2, \cdots, 100\}$ indicating the position of a heat source. In this work, we set $n = 20$.

Once having $\tilde{\boldsymbol{Y}}$, we transform it into another 0-1 sequence $\boldsymbol{Y}$ with length 100, which is defined as follows:

$$\forall i = 1, \cdots, 100, \ \boldsymbol{Y}_i = \begin{cases} 1, & \text{if } i \in \tilde{\boldsymbol{Y}} \\ 0, & \text{otherwise} \end{cases} \tag{5}$$

where $\boldsymbol{Y}_i = 1$ means position i of the predicted heat source layout design is placed with a heat source, and otherwise $\boldsymbol{Y}_i = 0$.

C. SAR MODEL TRAINING

In this part, we describe the architecture of the SAR model [35]. SAR mainly consists of two parts: a feature extractor and an attentive layout predictor. The extractor encodes the input image to various feature maps, and the predictor generates the heat source layout design by a novel 2D attention mechanism. The overall model structure is shown in Figure 6.

1) EXTRACTOR

The feature extractor is a 31-layer residual network (ResNet) [37]. Each residual block is either a 1×1 projection shortcut if the input and output dimensions are different, or an identity shortcut otherwise. All convolutional kernel size is 3×3 and all max-pooling size is 2×2. After passing through the extractor, the input image of the temperature field $\boldsymbol{X}$ is converted to various 2D feature maps, denoted as $\mathbf{V} \in \mathbb{R}^{H \times W \times D}$, where H is the height, W is the width and D is the number of channels.

2) PREDICTOR

The predictor is an attention-based sequence-to-sequence model. Both the encode and the decoder are long short term memory (LSTM) models. A novel 2D attention mechanism is used for capturing features of arbitrary shape and layout.

a: Encoder

Following [35], the encoder is a 2-layer LSTM model with 512 hidden state size per layer. At each step t, the encoder receives one column of $\mathbf{V}$ which results in a 2D tensor of shape $H \times D$, then followed by max-pooling along the vertical axis, thus giving a vector of length D. This vector is used to update the hidden state $\mathbf{h}_t$. After W steps, the final hidden state $\mathbf{h}_W$ is fed into the decoder for generating the

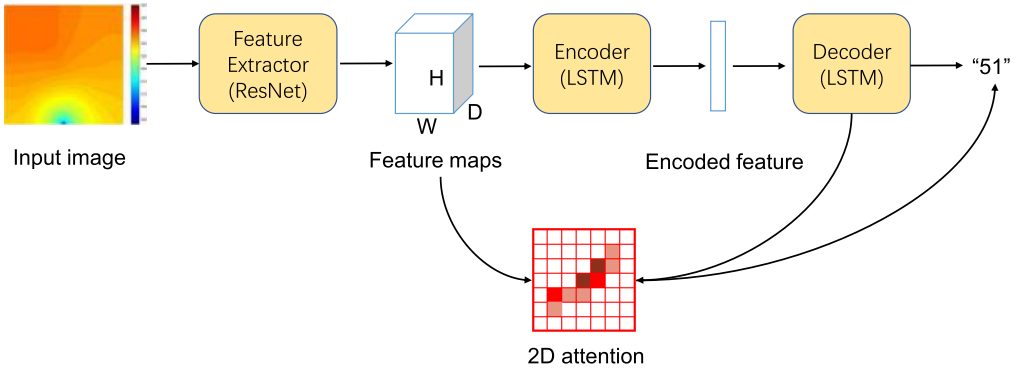

FIGURE 6. The architecture of show, attend and read model for inverse design. With a temperature field information given as the input, the output is a discrete sequence that represents the heat source layout.

layout design. The architecture of the encoder is shown in Figure 7.

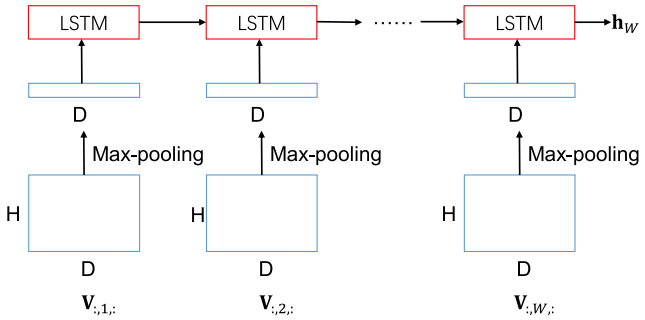

FIGURE 7. An illustration of the encoder.

b: Decoder

The decoder is also an LSTM model with 2 layers and 512 hidden state size of each layer. The decoder first receives the input $\mathbf{h}_W$ from the encoder, and then decodes a number at each step until generating a special [EOS] token. At step t, the decoded number y_t is in the range of [1, 100], which exactly indicates the positions in the layout. Therefore, the decoding process can be regarded as a classification task, where the total number of classes is 101, 100 numbers and a special [EOS] token.

More concretely, the inputs for each step are composed of two parts, the current hidden state $\mathbf{h}'_t$ and the output of the attention module g_t which will be introduced below. The result is obtained by a linear transformation and a softmax layer:

$$y_t = \text{softmax}(\mathbf{W}_o[\mathbf{h}'_t; \mathbf{g}_t]) \tag{6}$$

If $y_t \in \{1, 2, \cdots, 100\}$, then the process goes on, and if $y_t = [\text{EOS}]$, the decoding process finishes.

c: 2D Attention

The 2D attention mechanism aggregates local features so that neighborhood information are taken into account for finding the heat sources. The attention representation $\mathbf{g}_t$ is defined as follows:

$$\begin{cases} \mathbf{e}_{ij} &= \tanh(\mathbf{W}_v\mathbf{v}_{ij} + \sum_{p,q\in\mathcal{N}_{ij}} \tilde{\mathbf{W}}_{p,q}\mathbf{v}_{pq} + \mathbf{W}_h\mathbf{h}'_t) \\ \alpha_{ij} &= \text{softmax}(\mathbf{w}_e^{\mathrm{T}} \cdot \mathbf{e}_{ij}) \\ \mathbf{g}_t &= \sum_{i,j} \alpha_{ij}\mathbf{v}_{ij}, i = 1, \cdots, H; j = 1, \cdots, W \end{cases} \tag{7}$$

where $\mathbf{v}_{ij}$ is the feature representation at position (i, j) in $\mathbf{V}$, and $\mathcal{N}_{i,j}$ is the eight neighborhoods around this position. All $\mathbf{W}$ are learnable parameters.

3) LOSS FUNCTION DESIGN

We use the cross entropy error between the predicted layout position $\boldsymbol{Y}$ and real label $\hat{\boldsymbol{Y}}$ as the loss of the training process, which is simple but effective [38]. To ensure that the error could be calculated in cross entropy loss function. Both of $\boldsymbol{Y}$ and $\hat{\boldsymbol{Y}}$ are handled by the softmax operator. The loss is defined as the cross entropy error of the predicted value $\boldsymbol{Y}$ and the true value $\hat{\boldsymbol{Y}}$:

$$L(\hat{\boldsymbol{Y}}, \boldsymbol{Y}) = -\frac{1}{100}\sum_{i=1}^{100}[\log p(\boldsymbol{Y}_i)\hat{\boldsymbol{Y}}_i + \log(1 - p(\boldsymbol{Y}_i))(1 - \hat{\boldsymbol{Y}}_i)] \tag{8}$$

By combining the cross entropy loss and our predicted objective, we could successfully train SAR model and finally realize the purpose of predicting the heat source layout position.

The process of SAR is shown in Algorithm 1.

D. OPTIMIZATION PROCESS

In this section, taking the result predicted by SAR as the initial layout scheme, we design a simple but efficient optimization process to improve the accuracy. In our experiments, we find a scene that the temperature error between ground truth temperature field and predicted one by SAR would change severely around the local position of the heat source if predicted wrongly.

Then we take an example to illustrate the scene. We generate two heat source layout schemes. One is represented by{3, 7, 12, 18, 20, 22, 25, 28, 33, 34, 45, 46, 48, 55, 61, 63, 64, 65, 73, 84}, regarded as the ground truth. The other is encoded

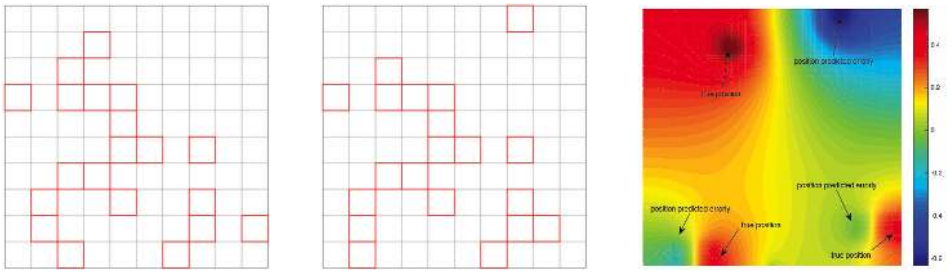

(a) Ground truth (b) Heat source predicted by SAR (c) The temperature error of two layout schemes

FIGURE 8. The temperature error when SAR could not predict all heat source layout.

Algorithm 1 The Training and Prediction Process of SAR

Input:
The raw temperature field $\boldsymbol{X}$ (and the ground-truth heat source layout $\hat{\boldsymbol{Y}}$ for training)
Output:
The predicted heat source layout $\boldsymbol{Y}$

```
Extracting feature maps: V ←extractor(X)
Encoding feature maps: h_W ←encoder(V)
Predicting heat source sequence: Ỹ ←Attentive Decoder(h_W)
Transforming to heat source layout using Eq. (5): Y ←Transform(Ỹ)
if training then
    Training SAR with Eq. (8)
end
else
    return Y.
end
```

as {2, 7, 12, 18, 19, 22, 25, 28, 33, 34, 45, 46, 48, 55, 61, 63, 64, 65, 73, 98}, regarded as the result predicted by SAR. Two schemes are visualized in Figure 8 (*a*) and (*b*). Figure 8 (*c*) displays the temperature field error of them.

As shown in Figure 8, there exists three heat source items not predicted rightly by SAR. However, form Figure 8 (*c*), we could observe that the temperature error shocks violently around the regions of true position and wrongly predicted ones. The temperature around the item predicted wrongly by SAR is lowest in the whole temperature error field. Conversely, the temperature around the item located in the ground-truth is highest in the whole temperature error field. It validates our observed scene. What's more, we also observation that the position of the highest temperature error in local region is corresponding to the position of ground truth one. The position of the lowest temperature error in local region is corresponding to the position of wrongly predicted one. Therefore, our main idea to optimize the layout scheme mainly includes two steps.

Step 1: Encode the temperature field and find the indexes of the positions of the highest temperature error and the lowest temperature error.

$$\begin{cases} \hat{y}_{max} = \lceil \frac{x_{error,max} \times 10}{L} \rceil + \lfloor \frac{y_{error,max} \times 100}{L} \rfloor \\ \hat{y}_{min} = \lceil \frac{x_{error,min} \times 10}{L} \rceil + \lfloor \frac{y_{error,min} \times 100}{L} \rfloor \end{cases} \tag{9}$$

where $(x_{error,max}, y_{error,max})$ and $(x_{error,min}, y_{error,min})$ stand for the coordinates of the highest temperature error and the lowest temperature error, $\lceil X \rceil$ rounds the elements of X to the nearest intergers towards infinity and $\lfloor X \rfloor$ rounds the elements of X to the nearest integers towards minus infinity.

Step 2: Correct the corresponding positions in the sequence standing for the predicted layout scheme Y_g.

$$\begin{cases} temp = Y_{g,\hat{y}_{max}} \\ Y_{g,\hat{y}_{min}} = temp \\ Y_{g,\hat{y}_{max}} = Y_{g,\hat{y}_{min}} \end{cases} \tag{10}$$

After above two steps, a new heat source layout scheme Y_g is predicted. Then we calculate the objective J. The optimization process would repeat the above steps until the stop criterion meets.

Combined with SAR with optimization process, our complete method is presented as Algorithm 2.

IV. EXPERIMENT

In this section, we conduct a series of experiments to testify the stability and feasibility of our proposed SAR-HSLID. In part IV-A, we conduct experiments on pre-generated test data to evaluate the accuracy of SAR model and study the relationship between the size of training data and the performance of model. Besides, to validate the extensiveness of our proposed method for inverse problem, we test the performance of SAR in unseen and extreme data. In part IV-B, based on the result predicted by SAR, we conduct experiments with optimization process. In part IV-C, considering in real world a large enough temperature field containing all points can be hardly get, we also conduct experiments using different sizes of temperature fields.

A. THE ACCURACY OF SAR MODEL

The SAR model is implemented in Intel(R) Core(TM) i7-8700 CPU @3.2GHz and 1 NVIDIA Tsela P100 GPU

Algorithm 2 The Proposed Inverse Method Based on SAR With Optimization (SAR-HSLID)

Input:
The initial input temperature filed $\boldsymbol{X_0}$, iteration number $t = 0$
Output:
The final multiple heat sources layout positions $\boldsymbol{Y}_g = \{y_{ig} = 0\text{or}1, i = 1, 2, \ldots, 100\}$

```
Use the SAR model to predict the heat source layout Y_0 according to Algorithm 1
Y_g = Y_0
Conduct the thermal simulation by FEM method using Y_g and obtain the temperature field X_p
while t < 20 do
    if J=0 then
        Return Y_g
    end
    Calculate the temperature filed error of X_0 and X_p, X_error = X_p - X_0
    Calculate the positions of highest temperature field error (x_error,max, y_error,max) and lowest temperature field error (x_error,min, y_error,min)
    Obtain the position of highest temperature field error ŷ_max, lowest temperature field error ŷ_min according to Eq. (9)
    Correct the value of the ŷ_max and ŷ_min position and update Y_g according to Eq. (10)
    Heat simulation, update X_p and calculate J according to Eq. (1)
    t = t + 1
end
Return Y_g
```

with 16G memory. We select Adam as the optimizer method. In the process of training, the batch size, the training epoch and the learning rate are set to 32, 50, 10^{-3}respectively. The data generated is listed in Table 1. In detail, 50000 general training samples and 5000 special training samples are generated respectively. In addition, we also generate 10000 general samples and 2000 special samples as the test data to validate the accuracy of SAR model. The high prediction accuracy reflects in that the layout inversely predicted by SAR should keep consistency with the expected one.

TABLE 1. The statistic of training and test data.

Data Type	Training		Test	
	General	*Special*	*General*	*Special*
Samples	50,000	5,000	10,000	2,000

To quantitatively evaluate the performance of SAR model, we design two criteria including Mean Accuracy (MA) and Mean Correct Ratio (MCR). For the predicted temperature field $\tilde{\boldsymbol{Y}}$ and the corresponding ground-truth one $\boldsymbol{Y}$, the Accuracy is defined as:

$$\text{Accuracy}(\tilde{\boldsymbol{Y}}, \boldsymbol{Y}) = \frac{n_{items}}{20} \tag{11}$$

where n_{items} stands for the number of heat source predicted rightly by SAR model in one single temperature field. And the Mean Accuracy is defined as:

$$\text{Mean Accuracy} = \frac{1}{N}\sum_{i=1}^{N}\text{Accuracy}(\tilde{\boldsymbol{Y}}, \boldsymbol{Y}) \tag{12}$$

where n_{items} stands for the number of heat source predicted rightly by SAR model in single temperature. And the Mean Correct Ratio is defined as:

$$\text{Mean Correct Ratio} = \frac{n_{samples}}{N} \tag{13}$$

where N is the total number of samples,and $n_{samples}$ is the number of samples predicted rightly by SAR, in which SAR model predicts all heat source items layout rightly.

We train the SAR model using general data, which is denoted by $\text{SAR}_{50\text{K}}$. We also train the SAR model using general data and special data together, which is denoted by $\text{SAR}_{50\text{K+SP}}$. Then we evaluate the performance of SAR model in general test data and special test data respectively. The statistical result is listed in Table 2. The validation performance of $\text{SAR}_{50\text{K+SP}}$ on general test data is illustrated in Figure 9.

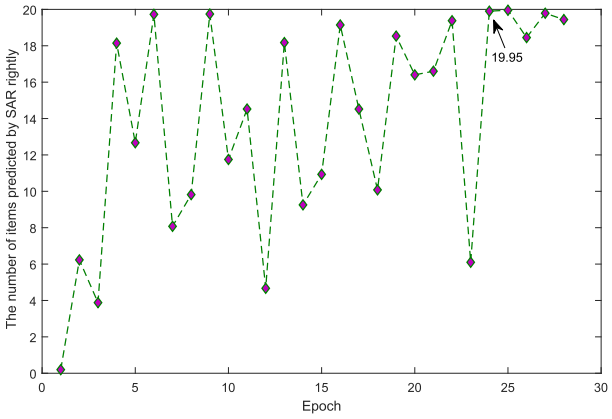

FIGURE 9. The validation performance of $\text{SAR}_{50\text{K}}$ on the general test data.

TABLE 2. The performance of $\text{SAR}_{50\text{K}}$ and $\text{SAR}_{50\text{K+SP}}$ on the test set.

Model	General Test		Special Test	
	MA(%)	MCR(%)	MA(%)	MCR(%)
$\text{SAR}_{50\text{K}}$	99.75	94.42	99.60	92.35
$\text{SAR}_{50\text{K+SP}}$	**99.90**	**98.81**	**99.70**	**93.24**

From Table 2, we could draw the conclusion that both of $\text{SAR}_{50\text{K}}$ and $\text{SAR}_{50\text{K+SP}}$ not only show superior performance in general test samples but also special test samples. The mean accuracy are all above 99%, which means that SAR could predict almost all heat source layout directly. In particular, the MA and MCR of $\text{SAR}_{50\text{K+SP}}$ could reach 99.90% and 98.81% on the general test. It means that SAR model could predict rightly all heat source layout in almost 4940 samples of 5000 samples totally. This testifies that adding the diversity of training data could help to improve the performance of model.

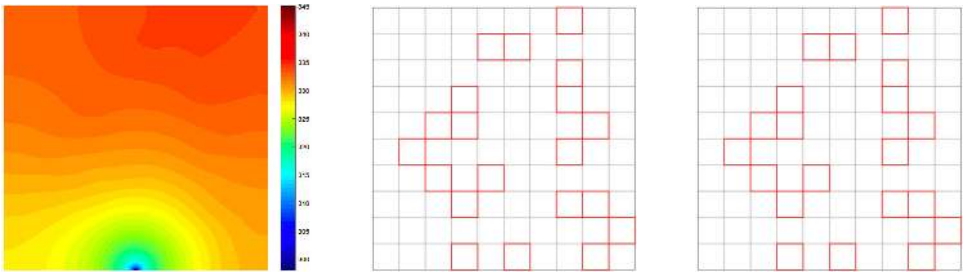

(a) Input temperature (b) Predicted layout (c) Ground truth

FIGURE 10. An illustration of the predicted heat source layout by using SAR_{50K} on one general temperature field sample (2). (a) the input temperature, (b) the predicted layout, (c) the ground-truth layout. (Temperature unit: K, the same below).

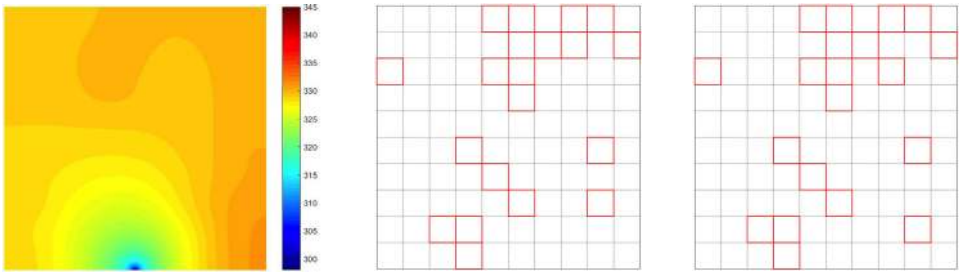

(a) Input temperature (b) Predicted layout (c) Ground truth

FIGURE 11. An illustration of the predicted heat source layout by using SAR_{50K} on one special temperature field sample (3). (a) the input temperature, (b) the predicted layout, (c) the ground-truth layout.

TABLE 3. Six samples selected as the test set, two drawn randomly from the general test set ((1) and (2)), two drawn randomly from the special test set ((3) and (4)) and two extreme test samples set ((5) and (6)).

NO.	MODEL	n_{items}	ACCURACY(%)
(1)	SAR_{50K}	19	95
(2)	SAR_{50K}	20	100
(3)	SAR_{50K}	18	95
(3)	SAR_{50K+SP}	20	100
(4)	SAR_{50K}	19	100
(4)	SAR_{50K+SP}	20	100
(5)	SAR_{50K}	11	55
(5)	SAR_{50K+SP}	15	75
(6)	SAR_{50K}	10	50
(6)	SAR_{50K+SP}	13	65

1) EVALUATING THE GENERAL TEST SAMPLE

To validate the generality of SAR model, we select two general samples to predict the corresponding heat source layout using SAR_{50K} model. The statistical result is listed in the first two row in Table 12. As shown in Figure 10, the input temperature field, predicted heat source layout and ground truth are also displayed.

According to the result, we can see that SAR_{50K} could predict accurately two general samples. For 20 heat source items layout positions, SAR_{50K} could predict out 19 and 20 respectively to two samples. The results of sample (2) are visualized in Figure 10, which validates the general performance of SAR model.

2) EVALUATING THE SPECIAL TEST SAMPLE

To study the influence of adding extra special data to the performance of SAR model, we use SAR_{50K} and SAR_{50K+SP} to predict two special samples selected by us respectively. The statistical result is listed in the thirdth to sixth row in Table 12. Compared with general samples, more heat source items are located in the around the wall of domain in special example (3) and special example (4). Therefore, some of the special test samples possess special temperature field, the layout of which is hard to predict. The results of two selected samples predicted by SAR_{50K+SP} are displayed in Figure 11 and Figure 12.

According to the statistical results, we could see that SAR_{50K} and SAR_{50K+SP} still could predict the special samples accurately. Particularly, SAR_{50K+SP} predict rightly the positions of all heat source items on both of two samples. In addition, the statistical results show that adding some special samples help to improve the performance of SAR model to some extent. On example (3), when SAR_{50K} could only predict 18 heat source items, the accuracy of SAR_{50K+SP} reaches 100%.

3) EVALUATING THE EXTREME TEST SAMPLE

To further test the performance of trained SAR model, we also take two extreme samples such as Figure 13(c) as the test samples. These two samples are not existed in any training set. In these two samples, 20 heat source items are all located in one corner of the domain. Therefore, the temperature

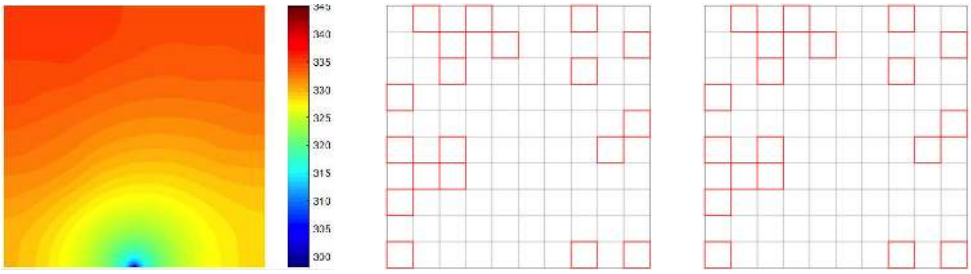

(a) Input temperature (b) Predicted layout (c) Ground truth

FIGURE 12. An illustration of the predicted heat source layout by using SAR_{50K+SP} on one special temperature field sample (4). (a) the input temperature, (b) the predicted layout, (c) the ground-truth layout.

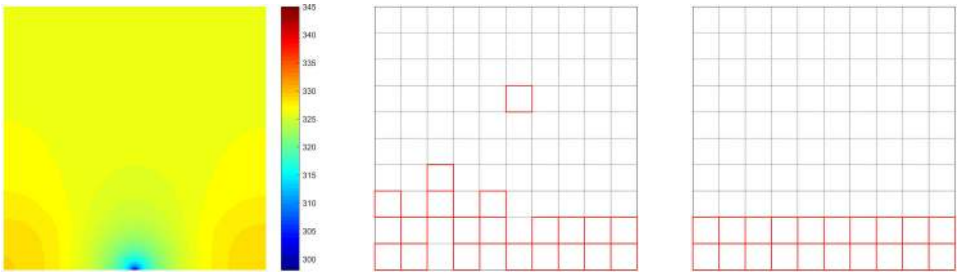

(a) Input temperature (b) Predicted layout (c) Ground truth

FIGURE 13. An illustration of the predicted heat source layout by using SAR_{50K+SP} on one extreme temperature field sample (5) not existed in any training data. (a) the input temperature, (b) the predicted layout, (c) the ground-truth layout.

fields are greatly different from previous ones in general test. We use SAR_{50K} and SAR_{50K+SP} to predict their layout giving the input temperature fields respectively. The statistical result is listed in the final four rows of Table 12. One of them is displayed in Figure 13.

According to the statistical results and Figure 13, we could see that SAR_{50K+SP} model still predict 75% heat source location and other heat source items predicted are very close to the ground truth, which means it intutively predicts out the heat source layout according to the trendency of the changing of temperature fileds. Apart from it, the accuracies of two samples predicted by SAR_{50K} model including special training data could reach 70% and 65% respectively. The above results show that the layout predicted by SAR model has been close to the ground truth even though being faced with the extreme layout schemes not existed in the training set.

Then, we investigate the relationship of the size of training data and the performance of SAR model. Motivated by the hope that using less data to train a well performing SAR model, we design an experiment. In detail, we select the training data randomly from 50,000 general training samples with fixed size. The size is fixed as 2k, 4k, 6k, 8k, 10k, 20k, 30k and 40k respectively, and corresponding trained models are denoted as SAR_{2K}, SAR_{4K}, SAR_{6K}, SAR_{8K}, SAR_{10K}, SAR_{20K}, SAR_{30K}, SAR_{40K} respectively together with previous SAR_{50K} and SAR_{50K+SP}. The statistical results are illustrated in Table 4. The error rates of predicted by different models are also displayed in Figure 14.

TABLE 4. Performances on the general test set and the special test set for different models.

MODEL	GENERAL TEST		SPECIAL TEST	
	MA(%)	MCR(%)	MA(%)	MCR(%)
SAR_{2K}	87.90	2.18	85.90	3.17
SAR_{4K}	94.05	18.65	92.75	16.70
SAR_{6K}	96.20	40.24	94.80	32.48
SAR_{8K}	96.70	47.28	96.05	43.03
SAR_{10K}	99.40	93.29	99.15	89.55
SAR_{20K}	99.75	16.92	99.20	18.44
SAR_{30K}	99.45	91.41	99.20	91.91
SAR_{40K}	99.60	92.22	99.20	90.06
SAR_{50K}	99.75	94.42	99.60	92.35
SAR_{50K+SP}	**99.90**	**98.81**	**99.70**	**93.24**

As shown in Table 4 and Figure 14, we could see that with more data, the predicted error rate decreased obviously. When the size of data is only 2k, the predicted accuracy could reach 87.9% and 85.9% on general test and special test respectively. However, the values of MCR are only 2.18% and 3.17%, which means that only few percentage of test data could be predicted rightly out all heat source positions. From Figure 14, when the size of data set reach above 10k, the error rate decreased below 1%. It validates that the data size has great influence on the performance of SAR model, though not better as larger as possible. In addition, the operation of adding extra special training data helps to improve the diversity of data. SAR_{50K+SP} achieves the best performance compared with other sizes of models. Apart from it, we observe that all SAR models has better performance on special test set

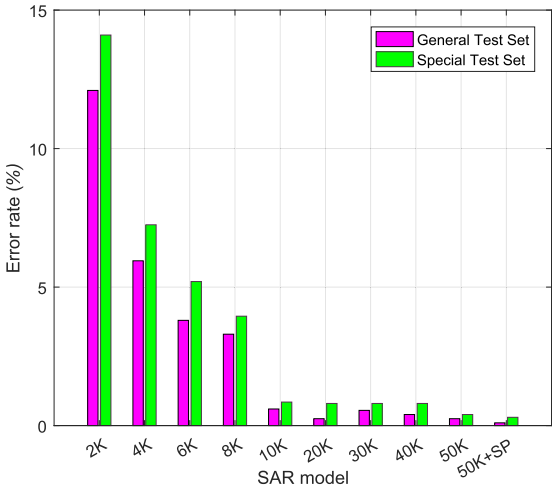

FIGURE 14. Performances on the general test set and the special test set for different models.

compared with special test set. It validates the generality of deep-learning based method.

B. THE PERFORMANCE OF THE SAR-HSLID FRAMEWORK

From above experiment results, we could see that SAR could predict almost all layout scheme rightly according to the input temperature field information. Aiming at the problem that for few samples SAR could not predict all heat source layout and that the accuracy of predicting extreme layout only reach to 50%, we continue to conduct experiments using SAR-HSLID to solve these challenges.

To evaluate the improvement of SAR-HSLID framework compared with pure SAR model, we add a metric called the number of mean thermal simulation (MTS), which is defined as follows:

$$\text{Mean Thermal Simulation} = \frac{n_{thermal}}{N} \tag{14}$$

where $n_{thermal}$ is denoted the number of thermal simulation needed in one sample using when SAR-HSLID finishes. In all the following experiments, the max iteration number is set as 20.

We conduct the process of optimizing the heat source layout based on the prediction of SAR_{50K} and SAR_{50K+SP}, which are denoted by SAR-HSLID_{50K} and $\text{SAR-HSLID}_{50K+SP}$ respectively. Two models are all tested on the general test and special test. The statistical result is illustrated in Table 5.

TABLE 5. The performance of SAR-HSLID_{50K} and $\text{SAR-HSLID}_{50K+SP}$ on the test set.

Model	General Test		Special Test	
	MA(%)	MTS	MA(%)	MTS
SAR-HSLID_{50K}	100	0.05	100	0.08
$\text{SAR-HSLID}_{50K+SP}$	100	**0.02**	100	**0.06**

According to Table 5, we see that both of SAR-HSLID_{50K} and $\text{SAR-HSLID}_{50K+SP}$ could predict rightly all heat source layout in general test and special test. Apart from it, both of the values of MTS are below 0.3, which means that SAR-HSLID method could predict all heat source layout rightly each time at the very low cost of heat simulation.

TABLE 6. Six samples selected as the test set, two drawn randomly from the general test set ((1) and (2)), two drawn randomly from the special test set ((3) and (4)) and two extreme test samples set ((5) and (6)).

No.	Model	$n_{thermal}$	Accuracy(%)
(1)	SAR-HSLID_{50K}	1	100
(2)	SAR-HSLID_{50K}	0	100
(3)	SAR-HSLID_{50K}	2	100
(3)	$\text{SAR-HSLID}_{50K+SP}$	0	100
(4)	SAR-HSLID_{50K}	1	100
(4)	$\text{SAR-HSLID}_{50K+SP}$	0	100
(5)	SAR-HSLID_{50K}	9	100
(5)	$\text{SAR-HSLID}_{50K+SP}$	5	100
(6)	SAR-HSLID_{50K}	10	100
(6)	$\text{SAR-HSLID}_{50K+SP}$	7	100

In addition, to compare with the predicted results of pure SAR model in part IV-A, we still select 6 samples same as Table 12. These six samples are predicted by SAR-HSLID_{50K} and $\text{SAR-HSLID}_{50K+SP}$ respectively. The results are illustrated in Table 6. Among 8 experiments, there exists three experiments not needing to conduct heat simulation. We study the relationship of the max temperature error and the iteration number on the other 5 experiments, which is displayed in Figure 16. The optimization processes of these experiments are also shown in Figure 15.

According to Table 5, we see that both of SAR-HSLID_{50K} and $\text{SAR-HSLID}_{50K+SP}$ could predict rightly all heat source layout in general test and special test. Apart from it, both of the values of MTS are below 0.3, which means that SAR-HSLID method could predict all heat source layout rightly each time at the very low cost of heat simulation.

As shown in Figure 16, for three general test samples namely 1-SAR(50K), 3-SAR(50K) and 4-SAR(50K), the max temperature error of them is only around 0.4K, 0.2K and 0.1K, which verifies the superior performance of SAR predictor. From the aspect of the cost of heat simulation, they just need 2 heat simulation at most. Apart from these, other four experiments on special samples not existed in training set are also displayed. The numbers of heat simulation of these four special samples are all below 10. In addition, we observe that the curve of the max temperature error is not decreasing alwaysly. It means that in the process of moving heat items, it might bring out severe temperature shock.

As shown in Figure 15, in our experiments, the lowest region of the temperature error field is where the wrong prediction by our SAR model. Conversely, the highest one is where the true position of one heat source. By showing their coordinates in the temperature error field, we could verify the basis observed by us that the regions of temperature error changing most severely are the location around the predicted wrongly heat source item and ground truth one.

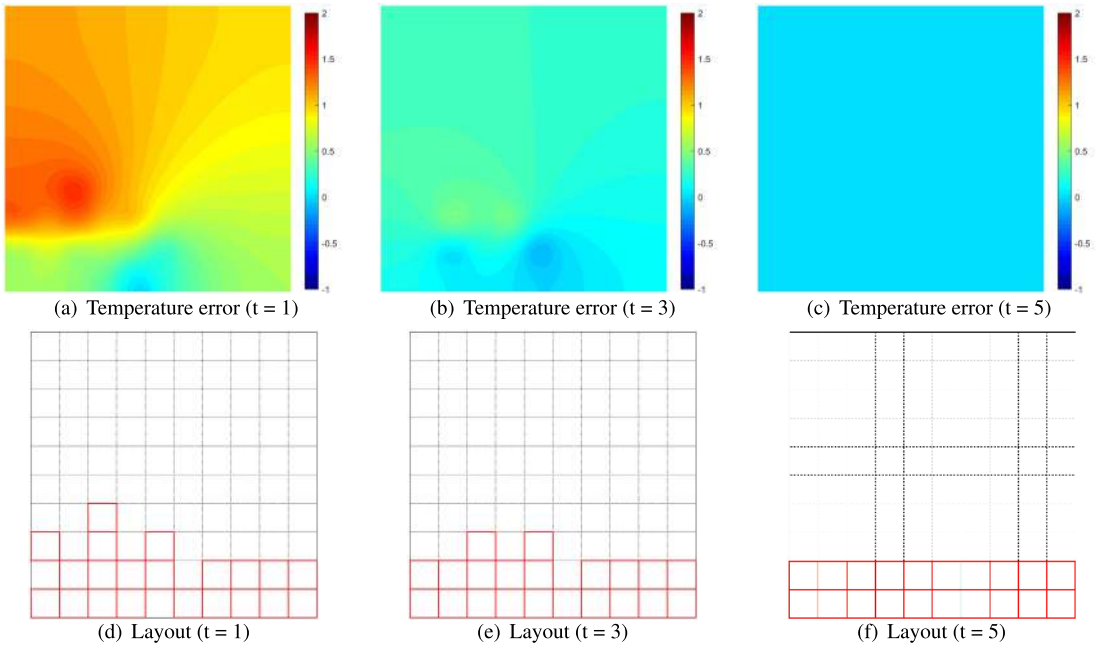

FIGURE 15. An illustration of the temperature error history with the iteration on the test sample (5) using the framework of SAR-HSLID$_{50K}$.

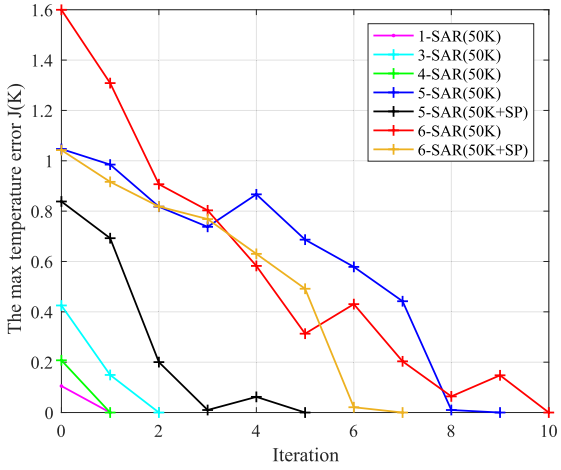

FIGURE 16. The max temperature error history with the iteration on the selected test samples using SAR$_{50K}$ and SAR$_{50K+SP}$ in the framework of SAR-HSLID.

C. THE PERFORMANCE OF SAR-HSLID USING DIFFERENT SIZES OF TEMPERATURE FIELD

In this part, to show the practicality of our proposed SAR-HSLID method, we conduct experiments on different size of temperature field. We utilize the operation MaxPool2d with kernel size 3, stride 1 and padding 1 to reduce the size of temperature field into half of the original. Then with the help of the operation of Upsample with bilinear mode, the temperature field could restore back double the size handled by the Mxpool2d. By this way, we investigate the relationship of the performance of SAR-HSLID method and the size of temperature field, namely 200×200, 100×100, 50×50 and 25×25. We evaluate the performance of SAR-HSLID$_{50K+SP}$ model on general test and special test handled by above operations. The statistical result is listed in Table 7.

TABLE 7. The performance of SAR-HSLID on the general test set and the special test set with different input temperature field size.

Model	General Test MA(%)	General Test MTS	Special Test MA(%)	Special Test MTS
SAR-HSLID(25×25)	100	4.75	100	5.50
SAR-HSLID(50×50)	100	2.21	100	2.40
SAR-HSLID(100×100)	100	0.81	100	1.13
SAR-HSLID(200×200)	100	**0.02**	100	**0.06**

As shown in Table 7, though the size of input temperature field is changed to smaller, the final mean accuracies of four model all reach 100%, which verifies the validation of our proposed SAR-HSLID framework for heat source layout inverse design. From the aspect of the number of needed heat simulation, the smaller input temperature field is reduced, the more heat simulation is needed. However, even though the temperature field size is reduced to 25×25 smaller than origin one, the number of needed heat simulation on general test and special test are just only 4.75 and 5.50 averagely.The numbers of required heat simulation for SAR-HSLID (100×100) and SAR-HSLID (50×50) are also only 2.21 and 0.81 respectively on the general test. In addition, we also select 2 samples randomly from the test set to verify the feasibility of four model. The results are illustrated in Table 8. Among 8 experiments, there needs to conduct at most four heat simulation. And they all could obtain the heat source layout schemes consisted with our expectation at last. It means that we could inversely design the heat source layout in practical complex

TABLE 8. Two samples selected as the test set, drawn randomly from the general test set ((1) and (2)).

No.	Model	$n_{thermal}$	Accuracy(%)
(1)	SAR-HSLID(25×25)	3	100
(1)	SAR-HSLID(50×50)	2	100
(1)	SAR-HSLID(100×100)	1	100
(1)	SAR-HSLID(200×200)	0	100
(2)	SAR-HSLID(25×25)	4	100
(2)	SAR-HSLID(50×50)	3	100
(2)	SAR-HSLID(100×100)	1	100
(2)	SAR-HSLID(200×200)	0	100

environments not only decreasing the number of heat simulation but also using temperature measurements as less as possible by using SAR-HSLID.

D. COMPARISION OF THE PROPOSED SAR-HSLID WITH THE TRADITIONAL OPTIMIZATION DESIGN METHOD

In above sections, we use the test data to verify the performance of SAR model. The calculations are based on cases where the temperature field corresponds to a known possible items distribution. In real application, the most ideal case is that designers could design this kind of temperature field according to their expectation such as reducing the max temperature or improving the uniformity of the layout domain.Then we could use SAR-HSLID directly to obtain the layout scheme. Considering the practical application, there exist some questions to be further discussed:

- How well does our method perform when using the near optimal temperature field obtained by optimization techniques as the input?
- How well does our method perform when using the relatively rough temperature field as the input?
- How well does our method perform compared with traditional methods when considering the computational cost?

In this section, two heat source layout optimization cases are utilized to answer the above questions. Case 1 demonstrates an unconstrained heat source layout optimization problem. The objective of this case is to identify the near optimal layout to reduce the maximum temperature of the layout domain. Case 2 demonstrates a constrained heat source layout optimization problem. In this case, the minimal temperature constraint on the special point needs to be satisfied simultaneously when minimizing the maximum temperature of the domain. For example, the temperature value in this special point cannot be less than a predefined level T_m, namely $T_{point} \geq T_m$ [26]. In case 2, the point is selected to $(0.1, 0.0561)m$ in the layout domain. T_m is set to 335K. All the following experiments are conducted in the same environment: Intel(R) Core(TM) i7-8700 CPU @3.2GHz and 1 NVIDIA Tsela P100 GPU with 16G memory.

We utilize the neighborhood search based layout optimization (NSLO) algorithm [26] to solve the above two cases.To handle the constraint in case 2, the penalty function method is adopted and then integrated with the objective function. The

TABLE 9. The statistic of time cost of two traditional methods in two heat source layout optimization cases. Single evaluation time denotes the time of heat simulation for one layout sample. Total time denotes the needed total time of optmization algorithm for solving the heat source layout optimization problem until the agorithm terminates.

Case	Method	Single evaluation time	Total time	T_{max}
Case 1	NSLO	0.3034s	2144.92s	326.75K
Case 2	NSLO	0.3034s	1638.18s	335.03K

TABLE 10. The statistic of time cost of our proposed method.

Number of data	Data preparation	Training	Inference
10,000	0.83h	1.51h	0.0464s
55,000	4.6h	8.32h	0.0464s

results of solutions are listed in Table 9. As we can see from Table 9, though the single evaluation time of heat simulation is only 0.3034s on average, the cost time of solving one case by optimization techniques is around 24 minutes. It is because that general optimization algorithm still needs thousands of number of objective function calculation to obtain the competitive heat source layout scheme. The heat source layout schemes optimized by them are visualized in Figure 17 and Figure 18.

Then we use the temperature fields optimized by the NSLO algorithm as the input of SAR_{50K+SP}. The predicted layout schemes are presented in Figure 17 and Figure 18. From aspect of the accuracy of our method, though the obtained temperature field by optimization is hardly seen in the training data, SAR model could predict 15 out of 20 heat sources in case 1. Particularly, SAR model could predict all 20 heat source rightly in case 2. From the aspect of time cost, the total time of our method including preparing 55,000 data and training the neural network is around 13h. The total time could be reduced to 2.33h if we only generate 10,000 samples as training data, the size of which has also posessed high prediction accuracy in Figure 14. It should also be noted that due to the independence among these samples, the computation cost of data preparation can be greatly relieved by parallel computing based on more CPU cores. Though the total time is much longer than traditional optimization methods if the data preparation and training time are added, the process of data preparation and training the neural network is one-shot. Moreover, the inference time of neural network is only 0.0464s. The cost would not increase too much with the layout design problem becoming complex because of treating it as an image-to-location task. Besides, faced with the same layout design problem, once the objective of optimization design is changed such as reducing the maximum temperature with some constraints in the special position of layout domain or improving the uniformity of temperature distribution simultaneously, the traditional optimization design method needs to repeat the optimization process, which brings out more cost. However, the additional cost of our method does not include the time od data preparation and

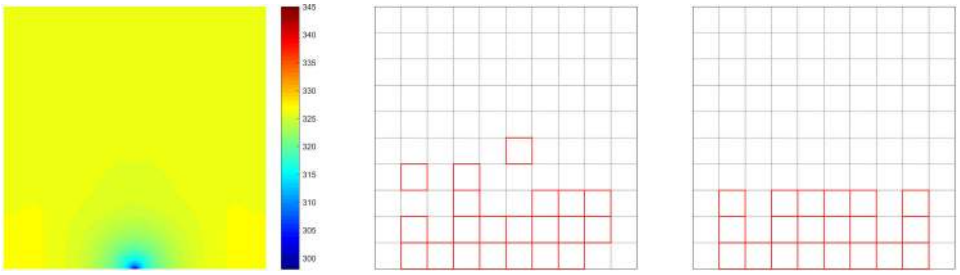

(a) Input temperature (b) Predicted layout (c) Ground truth

FIGURE 17. An illustration of the predicted heat source layout by using SAR_{50K+SP} on the obtained temperature field by optimization technique in case 1. (a) the input temperature of the near optimal layout, (b) the predicted layout, (c) the near optimal layout as the ground-truth layout.

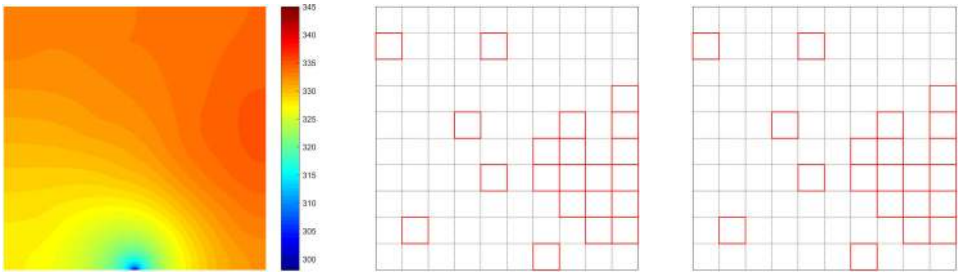

(a) Input temperature (b) Predicted layout (c) Ground truth

FIGURE 18. An illustration of the predicted heat source layout by using SAR_{50K+SP} on the obtained temperature field by optimization technique in case 2. (a) the input temperature of the near optimal layout, (b) the predicted layout, (c) the near optimal layout as the ground-truth layout.

training the neural network. It means that the advantages of reducing the computational cost of our method could be more remarkable compared with traditional optimization methods in this case.

To test the feasibility of our proposed method in real application, we deal with the temperature field by sampling less points or changing the values of each point to achieve a new temperature field as the input of SAR. In the first experiment, our operation is the same as section IV-C. Then we let SAR predict the new temperature field, the accuracy in two cases is listed in Table 11. Generally, SAR model could still predict competitive heat source layout when the input temperature field is changed to some extent. When only sampling 1/64 times number of points of the original one, the number of heat source being predicted wrongly is only reduced from 16 to 13, 20 to 17 respectively in two cases. Apart from it, in the second experiment, we change the value of each point of temperature field to generate a new one to further test the practicality of SAR. We take case 2 as an example. We introduce an offset of 20K in the original temperature picture. It could be seen that when the temperature fluctuates around 20K on the basis of the original one, the accuracy almost does not decrease. Even if the values are above 50K compared with the original temperature field, the number of predicted rightly heat sources is only reduced from 20 to 17. From the two experiments, we colud see that taking the relatively rough temperature field as the input, we could still obtain competitive heat source layout result. These could help to guide the easier construction of temperature field to realize the purpose of inverse design in real application.

TABLE 11. The performance of SAR with different input temperature field size on the two cases.

No.	Model	n_{items}	Accuracy(%)
Case 1	SAR(25×25)	13	65
	SAR(50×50)	13	65
	SAR(100×100)	14	70
	SAR(200×200)	16	80
Case 2	SAR(25×25)	17	85
	SAR(50×50)	18	90
	SAR(100×100)	19	95
	SAR(200×100)	20	100

TABLE 12. The performance of SAR with different input temperature field values on the two cases.

No.	Input temperature	n_{items}	Accuracy(%)
Case 2	$+50K$	17	85
	$+20K$	19	95
	$0K$	20	100
	$-20K$	20	100

V. CONCLUSION

In this article, the heat source layout inverse design problem is studied. Unlike the traditional numerical methods or evolutionary algorithms, we propose a novel framework based on deep learning named SAR-HSLID. The proposed method can effectively predict the heat source layout with greatly reduced simulation cost, which enables its wide applicability.

In our experiments, the mean prediction accuracy of SAR model could reach 99.9% on one test sample. In addition, based on the result predicted by SAR model, a simple but efficient method by use of the temperature error filed is proposed to make the final layout satisfy our required thermal performance, the accuracy of which could reach 100%. Besides, the relationship of the performance of SAR-HSLID and the size of input temperature field is also investigated. Experiments show that using less measurement points as the input, our proposed SAR-HSLID still derive competitive heat source layout with little heat simulation cost. These validate the feasibility and effectiveness of the proposed methodology in HSLID. Future research could conduct experiments on the more complicated circumstances such as the layout of multiple heat sources with different shapes or heat intensities and the construction of temperature field with high quality in real application.

REFERENCES

[1] D. W. Hengeveld, J. E. Braun, E. A. Groll, and A. D. Williams, "Optimal placement of electronic components to minimize heat flux nonuniformities," *J. Spacecraft Rockets*, vol. 48, no. 4, pp. 556–563, Jul. 2011.
[2] X. Chen, W. Yao, Y. Zhao, X. Chen, and X. Zheng, "A practical satellite layout optimization design approach based on enhanced finite-circle method," *Struct. Multidisciplinary Optim.*, vol. 58, no. 6, pp. 2635–2653, Dec. 2018.
[3] K. Chen, J. Xing, S. Wang, and M. Song, "Heat source layout optimization in two-dimensional heat conduction using simulated annealing method," *Int. J. Heat Mass Transf.*, vol. 108, pp. 210–219, May 2017.
[4] Y. Aslan, J. Puskely, and A. Yarovoy, "Heat source layout optimization for two-dimensional heat conduction using iterative reweighted L1-norm convex minimization," *Int. J. Heat Mass Transf.*, vol. 122, pp. 432–441, Jul. 2018.
[5] K. Chen, S. Wang, and M. Song, "Temperature-gradient-aware bionic optimization method for heat source distribution in heat conduction," *Int. J. Heat Mass Transf.*, vol. 100, pp. 737–746, Sep. 2016.
[6] A. Barnabas, E. Gabor, and L. Peter, "Inverse and algebraic quantum scattering theory," *Lect. Notes Phys.*, vol. 488, no. 1, p. 4, 1997.
[7] V. Mlinar, "Utilization of inverse approach in the design of materials over nano- to macro-scale: Utilization of inverse approach in the design of materials," *Annalen der Physik*, vol. 527, nos. 3–4, pp. 187–204, Apr. 2015.
[8] A. Jain, J. A. Bollinger, and T. M. Truskett, "Inverse methods for material design," *AIChE J.*, vol. 60, no. 8, pp. 2732–2740, Aug. 2014.
[9] O. Sigmund and K. Maute, "Topology optimization approaches," *Struct. Multidisciplinary Optim.*, vol. 48, no. 6, pp. 1031–1055, Dec. 2013.
[10] A. A. Egorov, "Inverse problem of theory of the laser irradiation scattering in two-dimensional irregular integrated optical waveguide in the presence of statistic noise," *Laser Phys. Lett.*, vol. 2, no. 2, pp. 77–83, Feb. 2005.
[11] C. E. Forest, "Quantifying uncertainties in climate system properties with the use of recent climate observations," *Science*, vol. 295, no. 5552, pp. 113–117, Jan. 2002.
[12] A. Poonawala and P. Milanfar, "Mask design for optical microlithography—An inverse imaging problem," *IEEE Trans. Image Process.*, vol. 16, no. 3, pp. 774–788, Mar. 2007.
[13] R. L. Johnston, "Evolving better nanoparticles: Genetic algorithms for optimising cluster geometries," *Dalton Trans.*, vol. 22, p. 4193, May 2003.
[14] N. S. Froemming and G. Henkelman, "Optimizing core-shell nanoparticle catalysts with a genetic algorithm," *J. Chem. Phys.*, vol. 131, no. 23, Dec. 2009, Art. no. 234103.
[15] M. B. Giles and N. A. Pierce, "An introduction to the adjoint approach to design," *Flow, Turbulence Combustion*, vol. 65, nos. 3–4, pp. 393–415, 2000.
[16] A. Krizhevsky, I. Sutskever, and G. Hinton, "ImageNet classification with deep convolutional neural networks," in *Proc. Adv. Neural Inf. Process. Syst.*, vol. 25, no. 3, 2012, pp. 1097–1105.
[17] R. Collobert, J. Weston, L. Bottou, M. Karlen, K. Kavukcuoglu, and P. Kuksa, "Natural language processing (almost) from scratch," *J. Mach. Learn. Res.*, vol. 12 pp. 2493–2537, Aug. 2011.
[18] J. R. R. Uijlings, K. E. A. van de Sande, T. Gevers, and A. W. M. Smeulders, "Selective search for object recognition," *Int. J. Comput. Vis.*, vol. 104, no. 2, pp. 154–171, Sep. 2013.
[19] M. Raissi, P. Perdikaris, and G. E. Karniadakis, "Physics informed deep learning (Part I): Data-driven solutions of nonlinear partial differential equations," 2017, *arXiv:1711.10561*. [Online]. Available: https://arxiv.org/abs/1711.10561
[20] M. Raissi, P. Perdikaris, and G. E. Karniadakis, "Physics informed deep learning (Part II): Data-driven discovery of nonlinear partial differential equations," 2017, *arXiv:1711.10566*. [Online]. Available: https://arxiv.org/abs/1711.10566
[21] A. Chug, S. Bhushan, and K. Mahajan, "HSI image restortion using low rank matrix recovery," *Int. J. Comput. Appl.*, vol. 117, no. 6, pp. 34–36, May 2015.
[22] I. Sosnovik and I. Oseledets, "Neural networks for topology optimization," *Russian J. Numer. Anal. Math. Model.*, vol. 34, no. 4, pp. 215–223, 2017.
[23] Y. Yu, T. Hur, J. Jung, and I. G. Jang, "Deep learning for determining a near-optimal topological design without any iteration," *Struct. Multidisciplinary Optim.*, vol. 59, no. 3, pp. 787–799, Mar. 2019.
[24] W. Chen, A. Jeyaseelan, and M. Fuge, "Synthesizing designs with interpart dependencies using hierarchical generative adversarial networks," in *Proc. 44th Design Autom. Conf.*, vol. 2A, Aug. 2018, pp. 1–16.
[25] Y. Zhang and W. Ye, "Deep learning–based inverse method for layout design," *Struct. Multidisciplinary Optim.*, vol. 16, no. 3, pp. 774–788, 2019.
[26] X. Chen, X. Chen, J. Zhang, and W. Yao, "The heat source layout optimization using deep learning surrogate modeling," *Struct. Multidisciplinary Optim.*, to be published.
[27] E. Hamouche and E. G. Loukaides, "Classification and selection of sheet forming processes with machine learning," *Int. J. Comput. Integr. Manuf.*, vol. 31, no. 9, pp. 921–932, Sep. 2018.
[28] J. Peurifoy, Y. Shen, L. Jing, Y. Yang, F. Cano-Renteria, B. G. DeLacy, J. D. Joannopoulos, M. Tegmark, and M. Solja ić, "Nanophotonic particle simulation and inverse design using artificial neural networks," *Sci. Adv.*, vol. 4, no. 6, Jun. 2018, Art. no. eaar4206.
[29] J. Peurifoy, Y. Shen, and L. Jing, "Nanophotonic inverse design using articial neural network," in *Proc. Frontiers Opt.*, 2017, Paper FTh4A.4.
[30] J. Tompson, K. Schlachter, P. Sprechmann, and K. Perlin, "Accelerating eulerian fluid simulation with convolutional networks," in *Proc. 5th Int. Conf. Learn. Represent. ICLR*, Toulon, France, Apr. 2017, pp. 3424–3433. [Online]. Available: OpenReview.net
[31] G. Kissas, Y. Yang, E. Hwuang, W. R. Witschey, J. A. Detre, and P. Perdikaris, "Machine learning in cardiovascular flows modeling: Predicting arterial blood pressure from non-invasive 4D flow MRI data using physics-informed neural networks," *Comput. Methods Appl. Mech. Eng.*, vol. 358, Jan. 2020, Art. no. 112623.
[32] M. Liu, L. Liang, and W. Sun, "Estimation of *in vivo* constitutive parameters of the aortic wall using a machine learning approach," *Comput. Methods Appl. Mech. Eng.*, vol. 347, pp. 201–217, Apr. 2019.
[33] Z. Han, Rahul, and S. De, "A deep learning-based hybrid approach for the solution of multiphysics problems in electrosurgery," *Comput. Methods Appl. Mech. Eng.*, vol. 357, Dec. 2019, Art. no. 112603.
[34] A. Agrawal, P. D. Deshpande, A. Cecen, G. P. Basavarsu, A. N. Choudhary, and S. R. Kalidindi, "Exploration of data science techniques to predict fatigue strength of steel from composition and processing parameters," *Integrating Mater. Manuf. Innov.*, vol. 3, no. 1, pp. 90–108, Dec. 2014.
[35] H. Li, P. Wang, C. Shen, and G. Zhang, "Show, attend and read: A simple and strong baseline for irregular text recognition," 2018, *arXiv:1811.00751*. [Online]. Available: https://arxiv.org/abs/1811.00751
[36] A. S. Reimer and A. F. Cheviakov, "A MATLAB-based finite-difference solver for the Poisson problem with mixed Dirichlet–Neumann boundary conditions," *Comput. Phys. Commun.*, vol. 184, no. 3, pp. 783–798, Mar. 2013.
[37] K. He, X. Zhang, S. Ren, and J. Sun, "Deep residual learning for image recognition," in *Proc. IEEE Conf. Comput. Vis. Pattern Recognit. (CVPR)*, Jun. 2016, pp. 770–778.
[38] H. Li, J. Niu, J. Chen, and H. Liu, "Entropy descriptor for image classification," in *Proc. 33rd Int. ACM SIGIR Conf. Res. Develop. Inf. Retr. SIGIR*, 2010, pp. 753–754.

JIALIANG SUN received the B.E. degree from the College of Aerospace Science and Engineering, National University of Defense Technology, Changsha, China, in 2018, where he is currently pursuing the M.E. degree. His research interests include evolutionary algorithms, deep learning, and satellite layout optimization design.

JUN ZHANG (Associate Member, IEEE) received the B.Eng. degree in aircraft systems and engineering and the M.Sc. degree in aeronautical and astronautical science and technology from the National University of Defense Technology, Changsha, China, in 2011 and 2016, respectively. He is currently pursuing the Ph.D. degree in computer science with the Department of Computer Science and Technology, Tsinghua University. He is an Assistant Professor with the Unmanned Systems Research Center, National Innovation Institute of Defense Technology. His research interests include Bayesian deep learning and adversarial examples.

XIAOYA ZHANG (Member, IEEE) received the M.Sc. and Ph.D. degrees from the College of Liberal Arts and Sciences, National University of Defense Technology, Changsha, China, in 2016 and 2020, respectively. She is currently an Assistant Professor with the Unmanned Systems Research Center, National Innovation Institute of Defense Technology. Her current research interests include machine learning, convex optimization, and combination optimization.

WEIEN ZHOU received the B.Sc. degree in mathematics from Nanjing University, Nanjing, China, in 2012, and the Ph.D. degree in computational mathematics from the National University of Defense Technology, Changsha, China, in 2017. He is currently an Assistant Professor with the Unmanned Systems Research Center, National Innovation Institute of Defense Technology. His research interests include numerical methods for stochastic systems, uncertainty quantification, and multidisciplinary design optimization.